Nanotechnology **20** (2009) 165705 (7pp) doi:10.1088/0957-4484/20/16/165705

On the structural and mechanical properties of Fe-filled carbon nanotubes—a computer simulation approach

G Soldano[1,2] **and M M Mariscal**[2]

[1] Institute for Theoretical Chemistry, Universität Ulm, D 89081 Ulm, Germany
[2] INFIQC, Unidad de Matemática y Física, Facultad de Ciencias Químicas, Universidad Nacional de Córdoba—5000 Córdoba, Argentina

E-mail: marmariscal@fcq.unc.edu.ar

Received 2 December 2008, in final form 3 March 2009
Published 1 April 2009
Online at stacks.iop.org/Nano/20/165705

Abstract
The structural and mechanical properties of single-and multi-walled carbon nanotubes filled with iron nanowires are studied using a recent parameterization of the modified embedded atom model. We have analyzed the effect of different crystal structures of iron (bcc and fcc) inside carbon nanotubes of different topographies. We have computed strain energy versus strain curves for pure systems: Fe nanowires, carbon and Fe-filled carbon nanotubes. A noticeable difference is found when these monatomic systems are joined to form iron-capped nanowires and where multi-layers of graphite are added to the nanotubes.

(Some figures in this article are in colour only in the electronic version)

1. Introduction

In recent years there have been numerous studies focusing on the insertion of 3d metals into carbon nanotubes (CNTs) [1–4]. In several experiments, nanowires have been prepared by encapsulating transition metals or ionic crystals inside nanotubes. It is expected that the atomic and electronic structures of interfaces between CNTs and metals play a major role in the mechanical, chemical and electronic properties of CNT composites. The filling of metals within CNTs has extended the potential application base of these materials to quantum memory elements, high density magnetic storage media, semiconducting devices, electron field emitters, high-resolution magnetic atomic force microscopy tips, magnetic field sensors, scanning probe microscopes and nanopipettes for metal transport [5–10]. Despite the diversity of metals available to be used for filling CNTs, Fe, Ni and Co have attracted special interest due to their ferromagnetic properties.

Different experimental approaches are often used to create metal-filled CNTs, generally with the same starting point, i.e. opening of the CNTs by the action of strong acids. Borowiak-Palen *et al* [11] have been able to fabricate Fe-filled single-walled carbon nanotubes (Fe-SWCNTs) by means of capillarity. Their preparation involves the immersion of the SWCNTs in an over-saturated solution containing $FeCl_3$ and subsequent washing with concentrated HCl. Finally, the sample is heated in air for 1 h at 593 K to decompose the $FeCl_3$ to iron and chlorine. Ferromagnetic behavior at room temperature with a hysteresis loop and large magnetic anisotropy was observed in those studies, indicating the formation of α-Fe(bcc) inside the CNT. Goldberg and co-workers [12] have carried out the synthesis of Fe-filled multi-walled carbon nanotubes (Fe-MWCNTs) by means of catalytic decomposition of ferrocene ($Fe(C_5H_2)_2$) in a quartz tube reactor. Using transmission electron microscopy (TEM) and high-resolution transmission electron microscopy (HRTEM) they were able to identify the structure of Fe inside the CNTs. Typically, standard crystal lattices, α-Fe(bcc), γ-Fe(fcc) and orthorhombic cementite (Fe_3C) were found inside the CNTs. Other experimental methods can be found in the literature for the fabrication of metal-encapsulated CNTs, such as wet chemistry [13], capillarity [14] and electrodeposition [15, 16], among others. Very recently, Jorge and co-workers [17] have been able to fabricate Fe-filled double-walled carbon

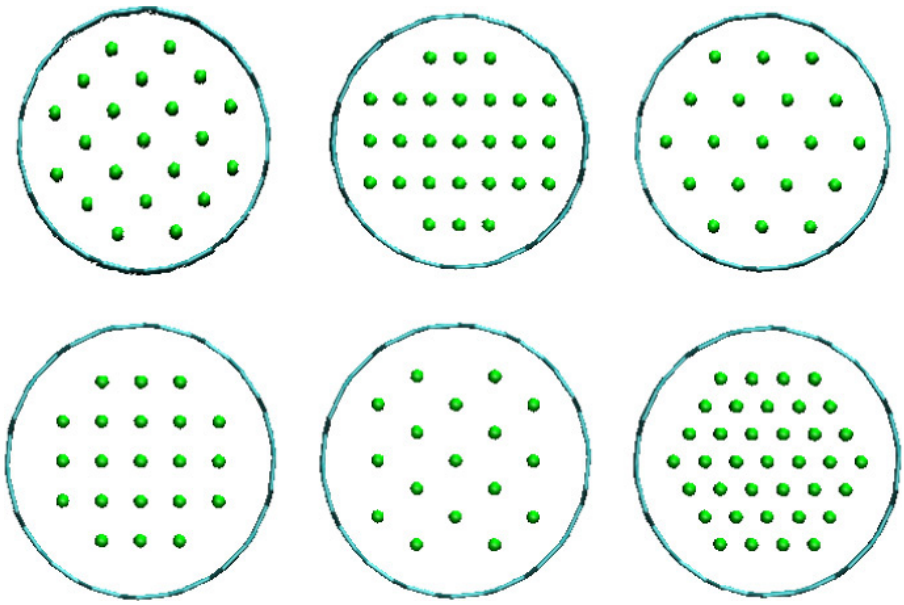

Figure 1. Top views of different initial configurations of Fe-filled SWCNTs. Upper panel (front left to right): bcc(100), (110) and (111). Lower panel (front left to right): fcc(100), (110) and (111).

nanotubes (Fe-DWCNTs) by means of capillarity and they report the presence of α-Fe nanowires (NWs) inside the DWCNTs.

In the present work, some mechanical and structural properties of pure CNTs, Fe-NWs and Fe-filled CNTs are studied by means of a combination of quenching dynamics simulations and energy minimization techniques employing the modified embedded atom method to describe the interaction between various atoms.

2. Models and methods

Quenching dynamics simulations and energy minimizations using the LBFGS quasi-Newtonian nonlinear optimization algorithm [18] were carried out in order to study some structural and mechanical properties of SWCNTs as well as MWCNTs filled with Fe-NWs.

It is well known that first-principles calculations provide the most reliable interatomic potentials for atomistic simulations; however, due to the size of the present system, it is not possible to study the behavior of materials within such approach. Alternatively, semi-empirical interatomic potentials dealing with more atoms can be used. It is interesting to note that the interatomic potential should be able to reproduce accurately various fundamental physical properties (elastic, structural, defect, thermal, surface properties, etc) of relevant elements and their alloys. For this purpose, several semi-empirical potentials have been developed for the Fe–C binary system. For instance, Johnson *et al* [19] and Rosato [20] reported interatomic potentials for the Fe–C system. However, both studies only addressed the behavior of single interstitial C atom in the Fe matrix, and did not consider the C–C interaction. More recently, Farkas and co-workers [21] reported a Fe–C semi-empirical potential in which they introduced the C–C interaction through the Tersoff potential. Ding *et al* [22] studied the initial stages of Fe-catalyzed nucleation and growth of SWCNTs where a combination of pair-wise and many-body potentials was used. Other theoretical studies [23, 24] used some kind of combinations rule, with a common formalism to treat the Fe–C interaction through pair potentials.

The modified embedded atom method (MEAM) potential is highly applicable to multi-component systems because it can describe the interatomic potentials of a wide range of elements (fcc, bcc, hexagonal close packed, diamond and even gaseous elements) using a common formalism and functional form. The MEAM was created by Baskes [25], by modifying the embedded atom method [26] to include the directionality of bonding. The method was subsequently modified by Lee and Baskes [27] to consider partially second-nearest-neighbor atom interactions.

In the MEAM, the total energy (E_t) of a system is given in the following form:

$$E_t = \sum_i E_i \qquad E_i = F_i(\bar{\rho}_i) + \tfrac{1}{2}\sum_{j(\neq i)} \varphi_{ij}(r_{ij}). \quad (1)$$

Thus, E_t is represented as the sum of the contributions of each atom. In equation (1), $F_i(\bar{\rho}_i)$ is the embedding energy required to embed an atom i in a local site with background electron density $\bar{\rho}_i$, and $\varphi_{ij}(r_{ij})$ is the pair interaction between atoms i and j separated by a distance r_{ij}. The background electron density at each atomic site is computed considering the directionality of bonding, i.e. by combining several partial electron density terms for different angular contributions with weight factors $t^{(h)}(h = 1\text{–}3)$. Each partial electron density is a function of the atomic configuration and atomic electron density. The atomic electron densities $\rho^{a(h)}(h = 0\text{–}4)$ are given as:

$$\rho^{a(h)}(r) = \rho_0 \exp\left[-\beta^{(h)}\frac{r}{r_{NN}-1}\right]$$

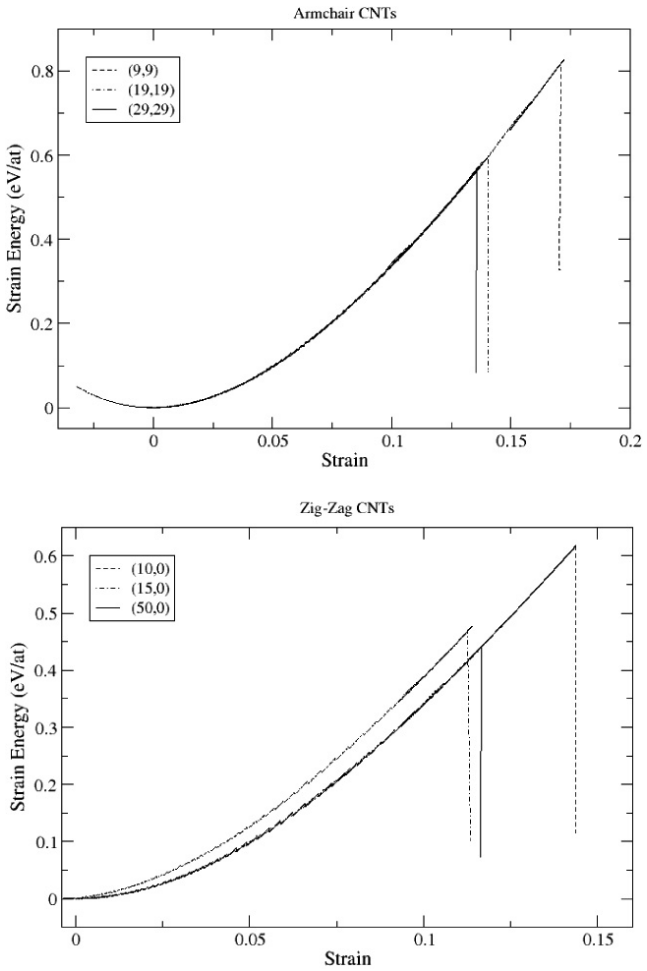

Figure 2. Strain energy versus strain curves for different (m, n)-SWCNTs. The upper panel shows armchair CNTs and the lower panel zig-zag CNTs.

where ρ_0 is the atomic electron density scaling factor, $\beta^{(h)}$, the decay lengths, are adjustable parameters, and r_{NN} is the nearest-neighbor distance in the equilibrium reference structure. A specific form is given to the embedding function F_i, but not to the pair interaction φ_{ij}. To describe the binary Fe–C interaction we have adopted the parameterization of Lee [28] carefully developed to reproduce diverse physical properties. In particular, this potential gives good agreement with fcc properties even though only bcc properties were used for fitting. It is well know that iron has quite a complex phase diagram which is mainly due to the magnetic properties of Fe, which influence the binding properties. Thus, we cannot claim that our study involves an accurate description of real Fe due to non-magnetic considerations; rather we use this system to study several mechanical properties of pure and encapsulated Fe-NWs.

In the present work we have performed computer simulations using different CNTs to evaluate the effect of nanotube chirality. The topography of SWCNTs is denoted by two numbers (n, m) which describe how graphite sheets roll up to form CNTs. SWCNTs with $n \neq 0$ but $m = 0$ are called zig-zag CNTs, $n = m$ are armchair CNTs, and the others are chiral CNTs. MWCNTs consist of multiple layers of graphite rolled in on themselves to form a tube shape.

Table 1. Formation energies (ΔE_{form}) and average distance between outer Fe atoms and the nanotube layer ($d_{\mathrm{Fe–C}}$) for Fe(bcc)-filled SWCNTs$_{(16,0)}$.

System	ΔE_{form} (eV)	$d_{\mathrm{Fe–C}}$ (Å)
Fe_{98}–SWCNT$_{(16,0)}$	−0.26	4.08
Fe_{182}–SWCNT$_{(16,0)}$	−0.32	2.40
Fe_{266}–SWCNT$_{(16,0)}$	−0.40	1.95

Using experimental methods such as TEM, HRTEM and x-ray diffraction, different crystal lattices of Fe, including α-Fe(bcc), γ-Fe(fcc), orthorhombic Fe_3C and hexagonal close packed NWs, were found to be formed inside the nanotubes [12, 29]. Therefore, on the basis of such experimental observations, we have constructed Fe-NWs with different structures oriented along [111], [110] and [100] crystallographic directions. With the same pure NW structures and CNTs we have constructed several kinds of Fe-filled CNTs. Top views of the initial configurations (before relaxation) of Fe-filled SWCNTs are shown in figure 1. Because of the lattice mismatch between the CNT and the bulk iron, the Fe atoms were allowed to relax to reach the same box length value. Periodic boundary conditions are applied on the axial direction while the others are held free.

Strain energy versus strain curves for pure CNTs, Fe-NWs and Fe-filled CNTs have been constructed using the LBFGS quasi-Newtonian nonlinear optimization algorithm. The tensile strain is applied by the reduction/enlargement of the computational cell in the axial direction. The stretching of the computational cell is carried out in small increments (10^{-4} Å) followed by energy minimization. Strain is obtained from $((L - L_0)/L_0)$, where L_0 and L are the tube lengths before and after the strain, respectively.

3. Results

First, we considered a single Fe atom adsorbed on the internal surface of a SWCNT. We performed quenching molecular dynamics and energy minimizations using the LBFGS quasi-Newtonian nonlinear optimization algorithm [18] to find relaxed structures. We found that a single Fe atom is placed above a hexagonal center, on energetic grounds, with an average bond distance of 0.206 nm, in very good agreement with recent first-principles calculations performed by Kang *et al* [30].

In order to determine the stability of Fe-filled SWCNTs, we calculated the formation energies (ΔE_{form}) as follows:

$$\Delta E_{\mathrm{form}} = \left[E_{\mathrm{Fe}_N\mathrm{CNT}} - \left\{E_{\mathrm{CNT}} + E_{\mathrm{Fe}_N}\right\}\right] N^{-1}$$

where $E_{\mathrm{Fe}_N\mathrm{CNT}}$ is the total energy of the system, E_{CNT} the energy of the pure nanotubes, E_{Fe_N} the energy of the Fe-NW and N the number of Fe atoms. Table 1 lists the values of formation energies and the average Fe–C distance for several systems, in which the number of Fe atoms inside a (16, 0)CNT was varied. As seen in the table, in all cases the

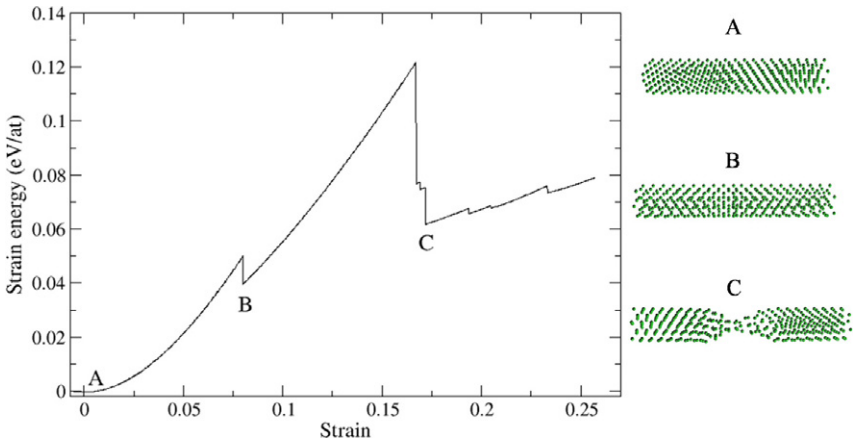

Figure 3. Left: strain energy versus strain curve for a bcc{111} Fe-NW. Right: atomic configurations at some characteristic points indicated on the curve.

Table 2. Formation energies (ΔE_{form}) for several Fe-filled multi-walled carbon nanotubes (nWCNTs(10, 0)).

System	ΔE_{form} (eV)
$Fe_{bcc(111)}$–1WCNT	−0.28
$Fe_{bcc(111)}$–2WCNT	−0.39
$Fe_{bcc(111)}$–3WCNT	−0.67
$Fe_{bcc(111)}$–4WCNT	−0.81
$Fe_{bcc(111)}$–5WCNT	−0.73

formation energy is negative, indicating that, from an energetic point of view, Fe-CNT systems are more stable than pure systems. A larger stabilization is observed when the nanotubes are 'completely' filled with iron (Fe_{266}–$SWCNT_{(16,0)}$ system), compared with recent density functional-tight binding (DFTB) calculations reported by Ivanovskaya *et al* [1] where, up to a certain limit, the filling of Fe-NWs is more energetically favorable than the encapsulation of clusters similar in size. In our calculations, the addition of more than 266 Fe atoms to the Fe_{266}–$SWCNT_{(16,0)}$ system leads to a positive value of ΔE_{form} in agreement with the results obtained by Ivanovskaya *et al*.

In order to evaluate the effect on the formation energy caused by the introduction of several sheets of graphite, we computed ΔE_{form} for four different systems in which the number of Fe atoms was kept constant. In table 2, the calculated values are shown for single- to four-walled CNTs filled with bcc Fe. In all cases, the formation energy is negative, and in general ΔE_{form} decreases with the number of graphite layers on the nanotube, indicating a stabilization of the binary system by the addition of several graphite layers. As stated by Ivanovskaya *et al* [1], these MWCNTs are more rigid than SWCNTs and the effects of the walls on curvature and deformation after wire encapsulation will be less pronounced and will therefore contribute to stabilizing the whole wire.

In a second series of simulations, strain energy versus strain curves for pure CNTs and Fe-NWs have been constructed using the LBFGS quasi-Newtonian nonlinear optimization algorithm in order to obtain the minimum energy configurations at each elongation step.

Figure 2 shows the strain energy versus strain curves for CNTs of different topographies and diameters: armchair and zig-zag ones. The curves evidence a similar elastic loading stage, characterized by monotonically increasing strain energy with increasing applied strain, followed by a yield point marked by a sudden drop in strain energy. A significant change in yield point is observed for CNTs of different diameters. For instance, the value of the critical strain increases as radius decreases, in good agreement with previous results [31]. A notable difference is also seen between the energy at the minimum (initial relaxed structure) and the final stage (after breaking), which can be attributed to the formation of two new surfaces perpendicular to the axial direction.

In order to determine the elasticity properties of pure Fe-NWs we have performed the same loading procedure. Figure 3 shows the strain energy versus strain curve for a α-Fe(bcc) NW with {111} crystalline planes perpendicular to the axial direction. A different behavior can be observed compared to the CNTs shown above. Initially, an elastic loading stage, characterized by monotonically increasing stress energy with increasing applied strain, is observed. At point B (see figure 3) a small strain-energy drop is characterized, which was recognized by a plastic deformation stage. Subsequently, a new elastic stage is observed until a small thin NW is formed. At this point, a new strain-energy drop is registered which corresponds to the breaking of the wire (see point C in figure 3). The atomic configurations for these characteristic points are plotted on the right-hand side of figure 3.

In figure 4, the energy versus strain curves are shown for pure Fe-NWs with both fcc and bcc structures. As expected, the α-Fe(bcc) NWs present a lower energy than that of the γ-Fe(fcc) structure. In all cases, the energy–strain curves show that elongation occurs through a sequence of elastic–plastic stages. Among the bcc structures, those with {100} plane were particularly unstable, and changed to a different configuration at the beginning of the elongation (see the jump in energy at 0 strain in figure 4).

The energy of this configuration rearrangement no longer responds quadratically in shape, but almost linearly with the increasing strain. The α-Fe NWs with a {110} plane do not reveal this rearrangement at the beginning of the elongation. However, they show a premature yield point compared to α-Fe NWs {111}. A relatively large energy drop

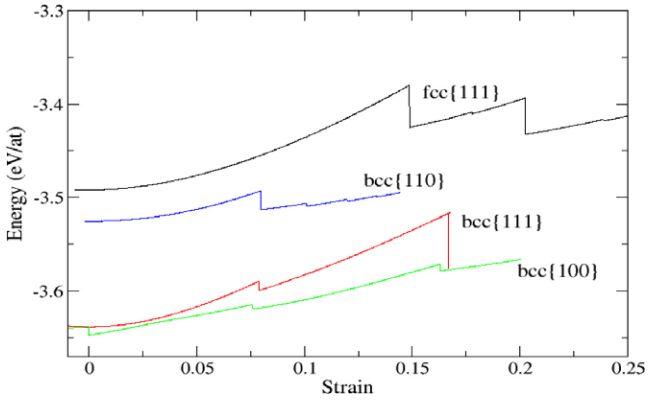

Figure 4. Energy versus strain curves for different Fe-NWs with several crystalline structures and crystallographic orientations.

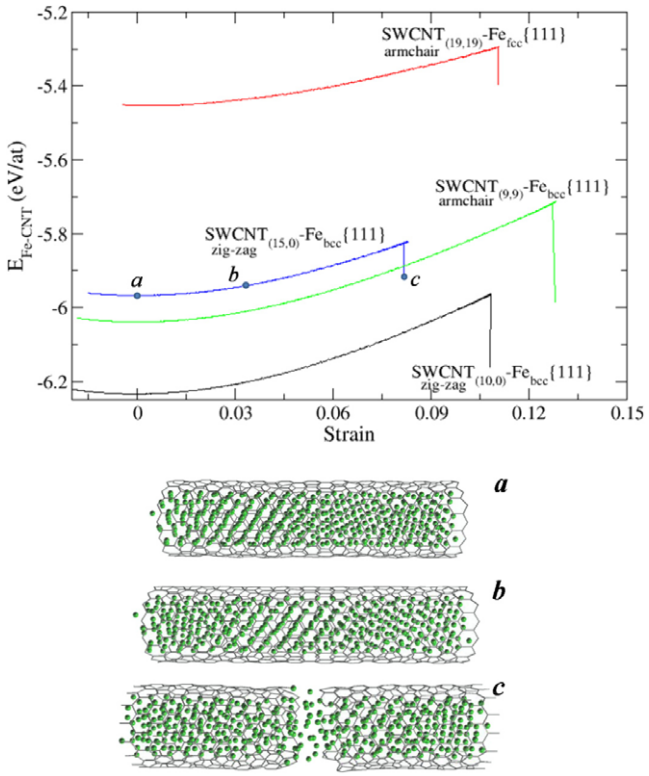

Figure 5. Upper panel: energy versus strain curves for different Fe-filled SWCNTs with diverse crystalline structures and orientations. Lower panel: atomic configurations at some characteristic points marked on the curve.

in plastic deformation is observed in the case of fcc(111) NWs. They were found to be due to strong atomistic reconfigurations, typically present during the elongation of compact surfaces [32].

In the case of Fe-filled CNTs, the elongation is dominated by the elasticity of the CNT. Figure 5 displays several energy–strain curves for different SWCNTs filled with both α-Fe(bcc$_{111}$) and γ-Fe(fcc$_{111}$). The zig-zag(10, 0) SWCNT filled with α-Fe(bcc$_{111}$) presents the lowest energy structure, in good agreement with pure materials. However, it also exhibits the lowest yield point as predicted for pure CNTs.

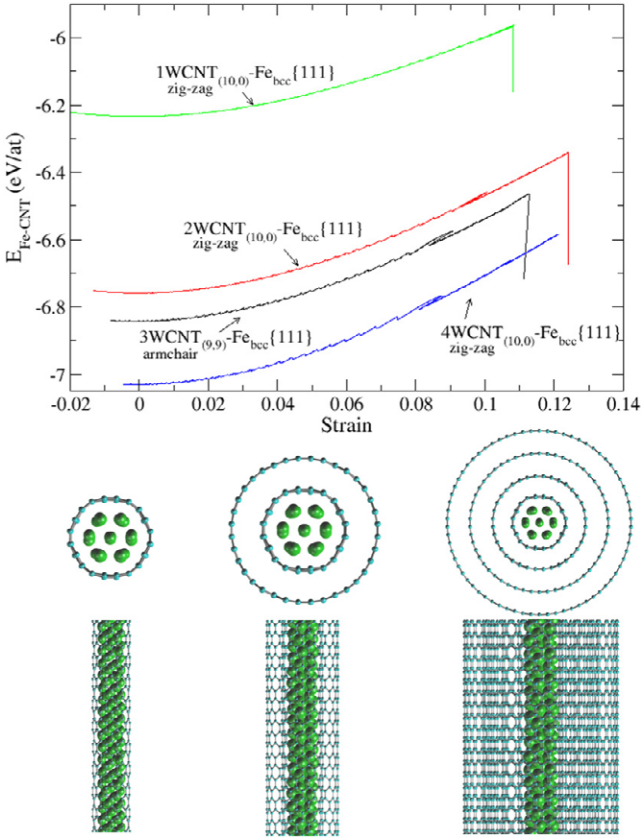

Figure 6. Upper panel: energy versus strain curves for different Fe-filled MWCNTs. Lower panel: top and front views of some atomic configurations of different MWCNTs at strain = 0. Note the distortion of the first nanotube sheet.

In all cases, the breaking point is determined by the rupture of the C bonds, and not by the Fe atoms. The energy–strain curves are characterized by a monotonically increasing energy with increasing applied strain, without any plastic deformation change, in contrast with the observations made for pure Fe-NWs. This can be explained by the impossibility of the configuration rearrangement imposed by the presence of the CNT surrounding the Fe wire. In figure 5 some characteristic atomic configurations are also plotted, which correspond to the zig-zag (15, 0) SWCNT filled with α-Fe(bcc$_{111}$). In frame (a), the initial (relaxed) structure shows a well-ordered bcc Fe-NW inside a SWCNT which does not present any deformation of buckling. In frame (b), a stage at strain $\sim$0.03 is shown in which the straining of the C bonds in the middle of the tube is evident. Finally in frame (c), the breaking CNT is observed; however, the Fe-NW is still bonded.

We have also performed simulations with MWCNTs filled with α-Fe(bcc$_{111}$). In figure 6, the energy versus strain curves are shown for CNTs with several layers (one to four) labeled 1WCNT to 4WCNT. From the figure it can be seen that the yield point does not change considerably in relation to the number of layers of the CNT. In order to quantify the structural rearrangements mentioned above during the loading stage, we have computed the pair distribution functions $g(r)$ for both α-Fe(bcc$_{111}$) NWs and α-Fe(bcc$_{111}$)-filled SWCNTs at the initial and final stages of the elongation process. In figure 7 the $g(r)$

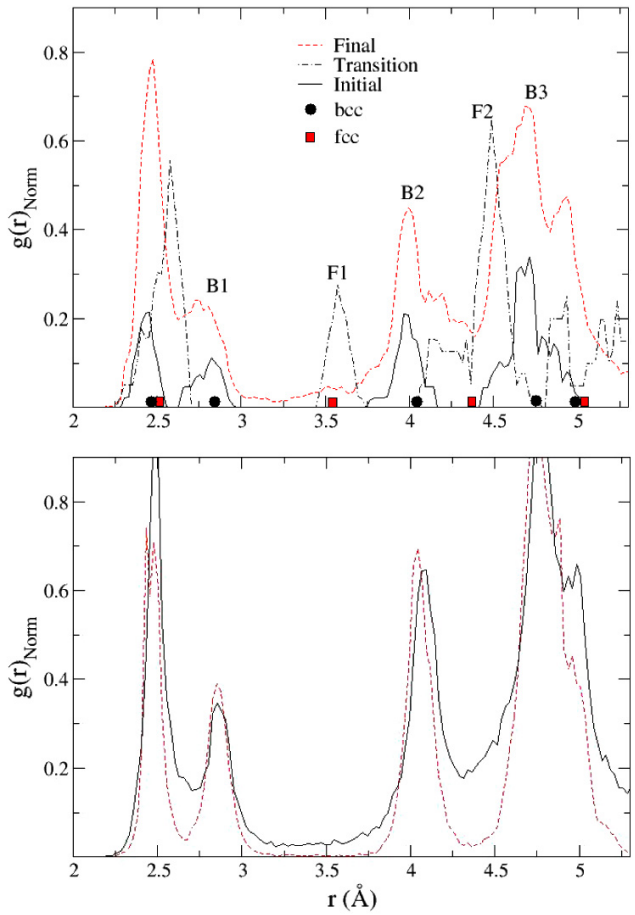

Figure 7. Pair distribution functions $g(r)$ of Fe atoms for a α-$Fe_{(bcc)}$ NW (upper panel) and α-$Fe_{(bcc)}$-filled $SWCNT_{(19,19)}$ (lower panel). The $g(r)$ function for the initial (relaxed) configuration is plotted with full line and the 'final' after rupture with a (on-line: red) dashed line. An intermediate stage during the elongation process of a pure Fe-NW is also plotted, which is labeled as 'Transition'. Note that the characteristic bcc (spheres) and fcc (squares) Fe–Fe distances of the bulk Fe $g(r)$ function are also plotted in the lower part of the figure and indicated as B1, B2, B3, F1 and F2.

functions are shown for Fe-NWs (upper panel) and Fe-filled SWCNTs (lower panel). The initial and final configurations are represented by full and dashed lines, respectively. The bcc and fcc Fe–Fe distances for bulk Fe are also plotted in the figure for comparison. As the plot illustrates for pure α-Fe(bcc_{111}) NWs, some characteristic γ-Fe(fcc_{111}) peak appears during the elongation procedure (see peak F1 and F2 in figure 7) whereas peak B1 disappears. These results reveal, in principle, the existence of a phase transition during the loading stage. In the case of Fe-filled SWCNTs, such a mechanism is not observed, and the α-Fe(bcc_{111}) remains unchanged during the whole loading stage.

4. Summary and conclusions

We present a computer simulation study of the mechanical and structural properties of Fe-NWs, CNTs and Fe-filled CNTs with different morphologies and crystalline structures. To the best of our knowledge this is the first time that the modified embedded atom method (MEAM) has been used to describe a metal-filled CNT system. This method describes accurately the many-body character of the metallic bond as well as the angularity in the C–C bonds.

Given the semi-empirical character of the MEAM method used in this paper, it is probable that our structural results differ somewhat from those that might be obtained using theoretically more accurate *ab initio* methods. In particular, our methods do not fully take into account the effects of electronic correlations on the magnetic behavior of the Fe–C system. However, since the MEAM is capable of describing the structural properties of a wide range of systems, we believe that our results must certainly reflect the general trends of the behavior of Fe/CNTs systems.

We have found that the addition of several layers of graphite to the CNT stabilized the binary system (Fe-CNT) compared to the SWCNTs.

For pure α-Fe(bcc_{111}) NWs, the strain energy versus strain curves together with the pair distribution functions reveal the possibility of a phase transition α-Fe(bcc_{111}) $\rightarrow$ γ-Fe(fcc_{111}) during the loading stage. This interesting observation constitutes a motivation for further research.

Acknowledgments

Authors wish to thank CONICET, Secyt UNC, Program BID 1728/OC-AR PICT no. 946 for financial support. We would like to thank E P Leiva for fruitful discussions and support and B-Joo Lee for assisting us in the understanding of the MEAM potential.

References

[1] Ivanovskaya V V, Köhler C and Seifert G 2007 *Phys. Rev.* B **75** 075410
[2] Grobert N *et al* 1999 *Appl. Phys. Lett.* **75** 3363
[3] Leonhardt A, Ritschel A, Kozhuharova R, Graff A, Mühl T, Huhle R, Mönch I, Elefant D and Schneider C M 2003 *Diamond Relat. Mater.* **12** 790
[4] Grobert N, Terrones M, Osborne A J, Terrones H, Hsu W K, Trasobares S, Zhu Y Q, Hare J P, Kroto H W and Walton D R M 1998 *Appl. Phys.* A **67** 595
[5] Liu J *et al* 1998 *Science* **280** 1253
[6] Wong E W, Sheehan P E and Lieber C M 1997 *Science* **277** 1971
[7] Saito S 1997 *Science* **278** 77
[8] Tans S J, Devoret M H, Dai H, Thess A, Smalley R E, Geerligs L J and Deeker C 1997 *Nature* **386** 474
[9] Hu J T, Min O Y, Yang P D and Lieber C M 1999 *Nature* **399** 48
[10] Svensson K, Olin H and Olsson E 2004 *Phys. Rev. Lett.* **93** 145901
[11] Borowiak-Palen E, Mendoza E, Bachmatiuk A, Rummeli M H, Gemming T, Nogues J, Skumryev V, Kalenczuk R J, Pichler T and Silva S R P 2006 *Chem. Phys. Lett.* **421** 129
[12] Golberg D, Mitome M, Müller Ch, Tang C, Leonhardt A and Bando Y 2006 *Acta Mater.* **54** 2567
[13] Jain D and Wilhelm R 2007 *Carbon* **45** 602
[14] Tan F Y, Fan X B, Zhang G L and Zhang F B 2007 *Mater. Lett.* **61** 1805
[15] Bao J C, Tie C Y, Xu Z, Suo Z Y, Zhou Q F and Hong J M 2002 *Adv. Mater.* **14** 1483

[16] Wang X H, Orikasa H, Inokuma N, Yang Q H, Hou P X, Oshima H, Itoh K and Kyotani T 2007 *J. Mater. Chem.* **17** 986
[17] Jorge J, Flahaut E, Gonzalez-Jimenez F, Gonzalez G, Gonzalez J, Belandria E, Broto J M and Raquet B 2008 *Chem. Phys. Lett.* **457** 347
[18] Nocendal J and Wright S J 1999 *Numerical Optimization* (New York: Springer) p 224
[19] Johnson R A, Dienes G J and Damask A C 1964 *Acta Metall.* **12** 1215
[20] Rosato V 1989 *Acta Metall.* **37** 2759
[21] Ruda M, Farkas D and Abriata J 2002 *Scr. Mater.* **46** 349
[22] Ding F, Bolton K and Rosén A 2004 *J. Phys. Chem.* **108** 17369
[23] Li H Y, Ren X B and Guo X Y 2007 *Chem. Phys. Lett.* **437** 108
[24] Wang L, Zhang H W, Zheng Y G, Wang J B and Zhang W Q 2008 *J. Appl. Phys.* **103** 083519
[25] Baskes M I 1992 *Phys. Rev.* B **46** 2727
[26] Foiles S M, Baskes M I and Daw M S 1986 *Phys. Rev.* B **33** 7983
[27] Lee B-J, Baskes M I, Kim H and Cho Y K 2001 *Phys. Rev.* B **64** 184102
[28] Lee B-J 2006 *Acta Mater.* **54** 701
[29] Jin-Phillipp N Y and Rühle M 2004 *Phys. Rev.* B **70** 245421
[30] Kang Y-J and Chang K J 2006 *Physica* B **376** 311
[31] Wang Y, Wang X, Ni X and Wu H 2005 *Comp. Mat. Sci.* **32** 141–6
[32] Mariscal M M, Narambuena C F, Del Pópolo M G and Leiva P M 2005 *Nanotechnology* **16** 974